Estimation of land surface albedo time series and trends based on MODIS data

Nikolaos Benas*, Nektarios Chrysoulakis
Foundation for Research and Technology - Hellas, Institute of Applied and Computational Mathematics, N. Plastira 100, Vassilika Vouton, 70013, Heraklion, Greece

ABSTRACT

The land surface albedo is among the most important parameters controlling the atmospheric radiation fluxes and the surface–atmosphere interactions. In the present study, surface albedo parameters and aerosol optical thickness (AOT) data from the Moderate Resolution Imaging Spectroradiometer (MODIS) sensor, onboard NASA's Terra and Aqua satellites, were analyzed and processed for the estimation of the shortwave surface albedo over Europe, Northern Africa and the Middle East, at 1 km × 1 km spatial resolution and on an 8–day average basis, for the period 2001–2012. The surface albedo was computed as a linear combination of black-sky and white-sky albedos. This methodology allows the computation of surface albedo for different values of AOT and solar zenith angle (SZA). MODIS Level 3 AOT data were used in the computations, while the surface albedo was calculated as an average of albedo values, using different SZAs on a pixel basis. The final albedo product was analyzed in terms of spatial and seasonal characteristics, and inter–annual trends, during the period examined. A strong dependency of the albedo on land cover type was found, as it was expected. The results also revealed substantial spatiotemporal variability of the surface albedo in the area examined, highlighting the great potential of satellite remote sensing in supporting climate change related studies, at both local and regional scales.

Keywords: Land surface albedo, MODIS, aerosol optical thickness, land cover, trends

1. INTRODUCTION

The land surface albedo (LSA) is defined as the ratio of the reflected solar radiation at the land surface to the total incoming solar radiation[1]. It is a critical physical variable, which affects the Earth's climate by controlling the planetary radiative energy budget and partitioning this energy between the atmosphere and the surface. Hence, measuring the LSA provides a quantitative means to investigate energy transfer between the land surface and atmosphere, and to better constrain regional and global climate modeling efforts[2]. LSA varies in space and time as a result of natural processes (e.g. solar illumination, snowfall and seasonal vegetation growth) and human activities (e.g. sowing and harvesting crops, urbanization), while abrupt changes are also often, caused primarily by forest fires[3]. These variations highlight two crucial aspects regarding the study of LSA: a) a continuous, global monitoring of its state and changes is required and using satellite remote sensing techniques for its derivation is the only feasible approach for fulfilling this requirement. b) The primary factor affecting LSA changes is corresponding Land Cover (LC) changes. Hence, evaluation of LSA changes and trends should be accompanied by assessment of LC changes. Various studies have highlighted the linkages between LSA and LC changes, focusing primarily on desertification, deforestation and reforestation, flooding, drought and urbanization[2].

Satellite multispectral observations are capable of deriving the spectral albedo, defined as the ratio between the hemispherical integrals of the up-welling (reflected) spectral radiance and the down-welling spectral radiance weighted by the cosine of the angle between the respective reference direction and the surface[4]. In general the spectral albedo of non-Lambertian surfaces depends on the angular distribution of the incident radiation - which in turn depends on the concentration and properties of scattering agents (e.g. aerosols) in the atmosphere and in particular on the presence of clouds. Therefore the spectral albedo is not a true surface property but rather a characteristic of the coupled surface-atmosphere system. For many applications the quantity of interest is not the spectral but rather the broad-band albedo which is defined as the ratio of up-welling to down-welling radiation fluxes in a given wavelength interval (e.g. shortwave). Given the spectral albedos, the average broadband albedos can be predicted under general atmospheric conditions using spectral-to-broadband coefficient[5].

Remote Sensing for Agriculture, Ecosystems, and Hydrology XVI, edited by Christopher M. U. Neale, Antonino Maltese, Proc. of SPIE Vol. 9239, 92390Q

Numerous LSA products have been and are being derived from satellite sensors, at a variety of spatial and temporal resolutions[2]. Among these sensors, MODIS, on board NASA's Terra and Aqua satellites, offers a continuous global dataset of parameters for the computation of LSA (explained in detail in Section 2.1) at a 16-day temporal resolution since 2000, and with spatial resolutions ranging from 0.5 km to 5 km[6].

In the present study, the time series of MODIS albedo parameters (spanning the period 2001-2012) was used for the calculation of the annual average LSA and its trends around the Mediterranean (including northern Africa, southern Europe and the Middle East) at 1 km × 1 km spatial resolution. Corresponding LC data from MODIS, covering the same period, were also used and analyzed for the quantification of the LC change effects on LSA trends. The wider Mediterranean area was selected due to its high climatic sensitivity; climate changes in the Mediterranean are already being observed, including decreasing precipitation and increasing high temperature extremes[7,8,9], and imminent desertification, foreseen by climatic projections[9].

In the next Section, the data and methodology used are described. These include the estimation of LSA using the MODIS parameters, estimation of LSA annual averages and trends, and analysis of the LSA trends relative to LC changes. Results are presented in Section 3, before the summary and conclusions.

2. DATA AND METHODOLOGY

2.1 LSA estimation

For the estimation of the LSA, the MODIS combined (from Terra and Aqua satellites) Bidirectional Reflectance Distribution Function (BRDF)/Albedo Model Parameters Product (MCD43B1) was used. This product is available on an 8-day basis and at 1 km × 1 km spatial resolution. It should be noted that the MODIS albedo model parameters are derived using observations from a 16-day period. Hence, although the product is available on an 8-day period, as already mentioned, successive 8-day products contain partially mutual information. In order to cover the entire area of interest (red rectangle in Fig. 1), 20 MODIS files are required for each 8-day period. All the files used in the present study (approx. 11,000), spanning the period 2001-2012, were downloaded from NASA's Land Processes Distributed Active Archive Center (LP DAAC).

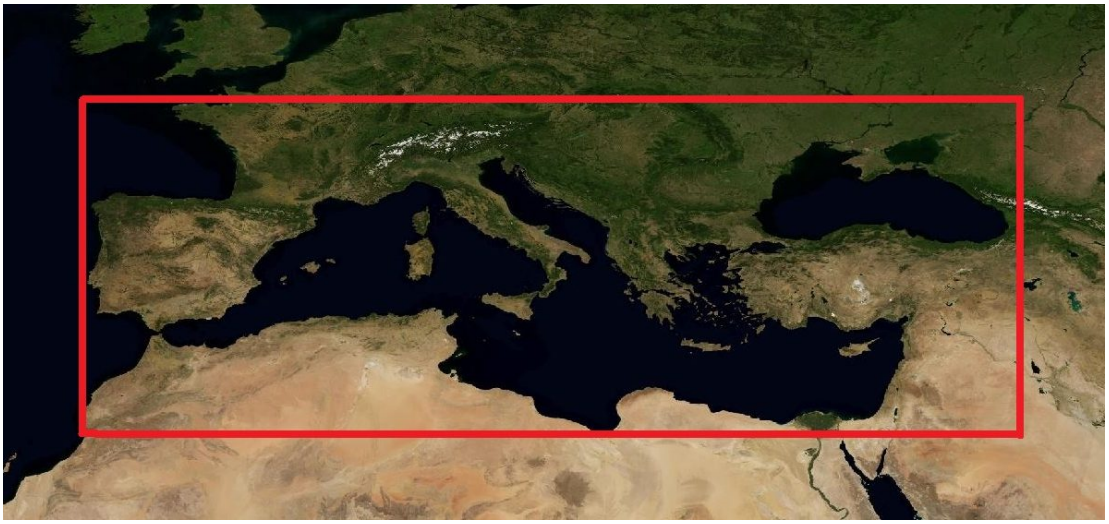

Figure 1. The wider Mediterranean study area, comprising southern Europe, northern Africa and the Middle East.

Among other parameters, the MCD43B1 product includes parameters for the computation of the directional-hemispherical surface reflectance (black-sky albedo) and the bi-hemispherical surface reflectance (white-sky albedo). Black-sky albedo is the limiting case of reflectance of a surface under direct illumination, while white-sky albedo is the limiting case of reflectance under diffuse illumination.

As discussed in a previous study[10], the BRDF can be expanded into a linear sum of terms (the so-called kernels), characterizing different scattering modes. The MODIS BRDF/Albedo algorithm makes use of a kernel-driven, linear BRDF model which relies on the weighted sum of an isotropic parameter and two functions (or kernels) of viewing and illumination geometry to determine reflectance[6]. The first of these kernels is the RossThick kernel and represents volumetric scattering from a dense leaf canopy based on a single scattering approximation of radiative transfer theory[11,12], and the second is the LiSparse kernel which is derived from the geometric-optical mutual shadowing model and assumes a sparse ensemble of surface objects[13]. The kernel weights, $f_k(\lambda)$, are selected from those that best fit the available observational data. Their derivation, i.e., the process of model inversion, is achieved through a fitting procedure that tunes the model to observed data points by minimizing mean square residuals. These weights are available on a pixel basis in MCD43B1 products, separately at seven wavelengths (470, 550, 660, 865, 1240, 1640 and 2130 nm) and three broad bands (0.4-0.7, 0.7-4.0 and 0.25-4.0 μm). Hence, using these weights, the black-sky and white-sky albedos (α_{bs} and α_{ws}, respectively), were calculated using the following polynomial[6]:

$$\alpha(\theta,\lambda) = f_{iso}(\lambda)(g_{0iso} + g_{1iso}\theta^2 + g_{2iso}\theta^3) + f_{vol}(\lambda)(g_{0vol} + g_{1vol}\theta^2 + g_{2vol}\theta^3) + \\ + f_{geo}(\lambda)(g_{0geo} + g_{1geo}\theta^2 + g_{2geo}\theta^3)$$

Where θ is the solar zenith angle, λ the wavelength, and g_{kj} are coefficients, listed in a previous study[6]. In the present study, the broad band (0.25-4.0 μm) albedos were estimated.

To obtain an approximation of the albedo for ambient illumination conditions (blue-sky albedo), it is suggested[4,14] to linearly combine the white-sky albedo and the black-sky albedo. The diffuse component then can be expressed as a function of wavelength, optical depth, aerosol type, and terrain contribution. Therefore, for partially diffuse illumination, the actually occurring albedo (blue-sky albedo) value may be approximated as a linear combination of the limiting cases[6]:

$$\alpha(\theta,\lambda) = \{1 - S(\theta,\tau(\lambda))\}\alpha_{bs}(\theta,\lambda) + S(\theta,\tau(\lambda))\alpha_{ws}(\theta,\lambda)$$

Where $\tau(\lambda)$ is the aerosol optical thickness (AOT) and $S(\theta,\tau(\lambda))$ the fraction of diffuse radiation. Values of $S(\theta,\tau(\lambda))$ are retrieved from a look-up table (LUT), based on θ and $\tau(\lambda)$ [6].

For the LSA (blue-sky albedo) estimation, data of the AOT at 550 nm from MODIS Level 3 products, also available on an 8-day mean basis and at 1° × 1° latitude-longitude resolution, were retrieved for the same period, separately from Terra and Aqua satellites. For each 8-day, the average Terra and Aqua MODIS AOT was estimated and linearly interpolated to coincide with the 1 km × 1 km LSA spatial resolution. For each pixel and 8-day, the LSA was estimated at four different solar zenith angles, corresponding to 9:00, 12:00, 15:00 and 18:00 local time of the first of the eight days. The 8-day LSA was computed as the average of these four values.

2.2 Estimation of the annual average LSA

The optimum estimation of the annual mean LSA on a pixel basis can be achieved by averaging the 8-day means (approximately 46 in one year), additionally ensuring that all 8-day means are present in the computation. This is not always the case in satellite-derived products, since several reasons can cause failures in retrieval algorithms and consequent gaps in time series. In the case of the LSA retrieval, the main reason for gaps is the presence of clouds, which is exacerbated especially in higher latitudes and during winter months. Hence, for a meaningful and uniform estimation of LSA annual averages, the following control thresholds were defined: a) at least 23 (out of 46) 8-day averages were required for the computation of the annual mean; and b) to avoid annual albedo biases towards summer values, since clear sky days prevail during this season, an additional threshold regarding the temporal homogeneity of 8-day LSAs was applied, accepting a maximum number of four successive missing 8-day LSA values. In each pixel where the above mentioned criteria were met, the smoothing spline technique was used to fill the missing 8-day values and compute the corresponding annual mean LSA. This approach was selected based on the findings of a previous study[15], which showed that, among several gap-filling and smoothing methods of datasets with seasonal patterns and winter or summer gaps, the smoothing spline technique produces the best fit to the original data, while it does not introduce spurious or intermittent features.

2.3 Calculation of LSA trends

The investigation of LSA changes during the 12–year period examined was based on the calculated annual averages; a linear regression analysis was performed on a pixel level and the LSA change was calculated in %, based on the slope of the linear regression equation. In order to ensure the representativeness of these changes, a threshold of at least 10 (out of 12) annual mean values was applied. Furthermore, annual mean LSA in the first (2001) and last (2012) year of the time series was required, to ensure the homogeneity in trends regarding the period covered. Statistically significant trends at the 95% confidence level were also identified on a pixel level, based on the lower and upper confidence bounds of the retrieved linear regression slope: a trend is statistically significant if the interval defined by these bounds does not contain zero.

2.4 Estimation of LSA trends relative to LC changes

Land cover type data were acquired from the MODIS Land Cover Type product. This product contains five classification schemes, which describe land cover properties derived from MODIS one-year observations from both Terra and Aqua. In the present study, the primary land cover scheme was used, which identifies 17 land cover classes defined by the International Geosphere Biosphere Programme (IGBP), including 11 natural vegetation classes, 3 developed and mosaicked land classes, and three non-vegetated land classes[16]. The 17 land cover types are shown in Table 1. The product is available on an annual basis and at 500 m × 500 m spatial resolution.

For the assessment of LSA trends relative to LC changes, LC type data of the first (2001) and last year (2012) of the study period were retrieved. These data were first collocated with the LSA data by upscaling from their initial resolution (500 m × 500 m) to the LSA resolution (1 km × 1 km) using a majority criterion: in each LSA pixel, the LC type that occupied the majority of the 4 corresponding LC pixels was assigned.

Having the LSA calculated on a pixel basis (Section 2.3), average LSA trends were estimated for pixels in which any of the 16 × 16 possible land cover changes was observed between 2001 and 2012 (these combinations include pixels with unchanged LC types, but exclude water surfaces).

3. RESULTS

3.1 Average LSA

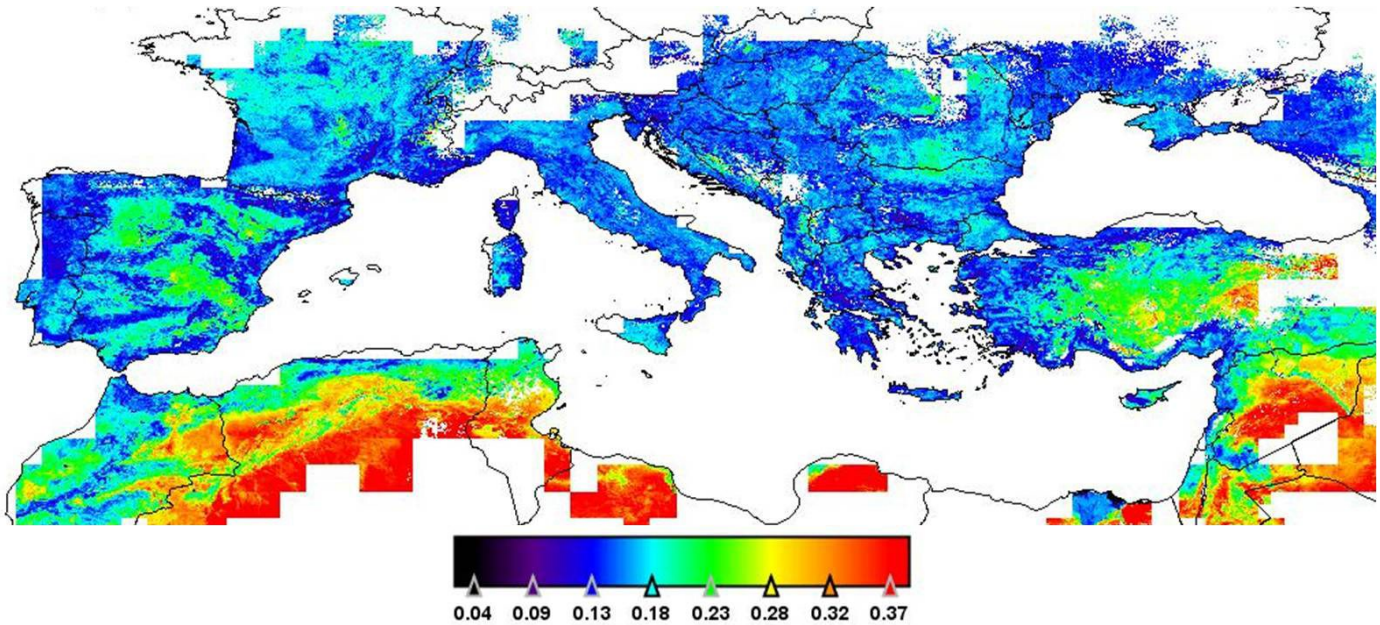

Figure 2. Spatial distribution of the LSA at the study area, computed as the average of the annual mean values.

Figure 2 shows the spatial distribution of the average LSA, computed from the corresponding annual mean values during the period examined. The highest LSA values, exceeding 0.4 in large areas, occur in desert regions of northern Africa (Sahara desert) and the Middle East. Patches of high albedo values are also apparent in mountainous areas (e. g. the Alps), due to the domination of snow cover and of barren areas in high altitudes. In the majority of the southern European areas, on the other hand, LSA values range between about 0.15 and 0.25. Minor gaps in the image should be attributed to pixels not meeting the threshold criteria described in Section 2.2, while major no-data areas are due to missing AOT values, which is available at 1° × 1° spatial resolution.

In Table 1, spatially averaged values of LSA, and their corresponding standard deviations, are given for each LC type. LC types of 2012 were used for these computations. These averages confirm that the highest LSA values appear in barren areas, especially deserts, reaching 0.33 on average. It should be noted, however, that these averages do not reveal the high seasonal LSA variation of several LC types (e.g. croplands), but can be considered representative of LC types which do not vary seasonally (e.g. urban/built-up areas, deserts). Snow and ice LSA is not given in Table 1, due to the insufficient number of corresponding pixels, which vary considerably in both space and time.

Table 1. The 17 land cover types used and the corresponding average (±1σ) LSAs, computed from the entire study area and time series.

Type number	**Land Cover Type**	**Average LSA (±1σ)**
0	Water	-
1	Evergreen Needleleaf forest	0.12 ± 0.03
2	Evergreen Broadleaf forest	0.14 ± 0.02
3	Deciduous Needleleaf forest	0.11 ± 0.04
4	Deciduous Broadleaf forest	0.14 ± 0.01
5	Mixed forest	0.13 ± 0.02
6	Closed shrublands	0.12 ± 0.02
7	Open shrublands	0.22 ± 0.05
8	Woody savannas	0.14 ± 0.02
9	Savannas	0.15 ± 0.02
10	Grasslands	0.21 ± 0.06
11	Permanent wetlands	0.09 ± 0.03
12	Croplands	0.18 ± 0.03
13	Urban and built-up	0.16 ± 0.03
14	Cropland/Natural vegetation mosaic	0.16 ± 0.02
15	Snow and ice	-
16	Barren or sparsely vegetated	0.33 ± 0.06

3.2 Spatial distribution of LSA trends

In Figure 3, the spatial distribution of the LSA trends (in %) during the period examined, is presented. While the thresholds applied in the trends calculations (Section 2.3) create large gaps in the map, some general characteristics are apparent: decreasing LSA trends dominate in both NW Africa and the Iberian Peninsula, while large areas of increasing LSA appear in south France and the Middle East, where in several regions the albedo has increased by over 10%. In

Italy, Greece and Turkey, trend signs are mixed, and vary between small neighboring regions. These variations should probably be attributed to local land cover characteristics and changes.

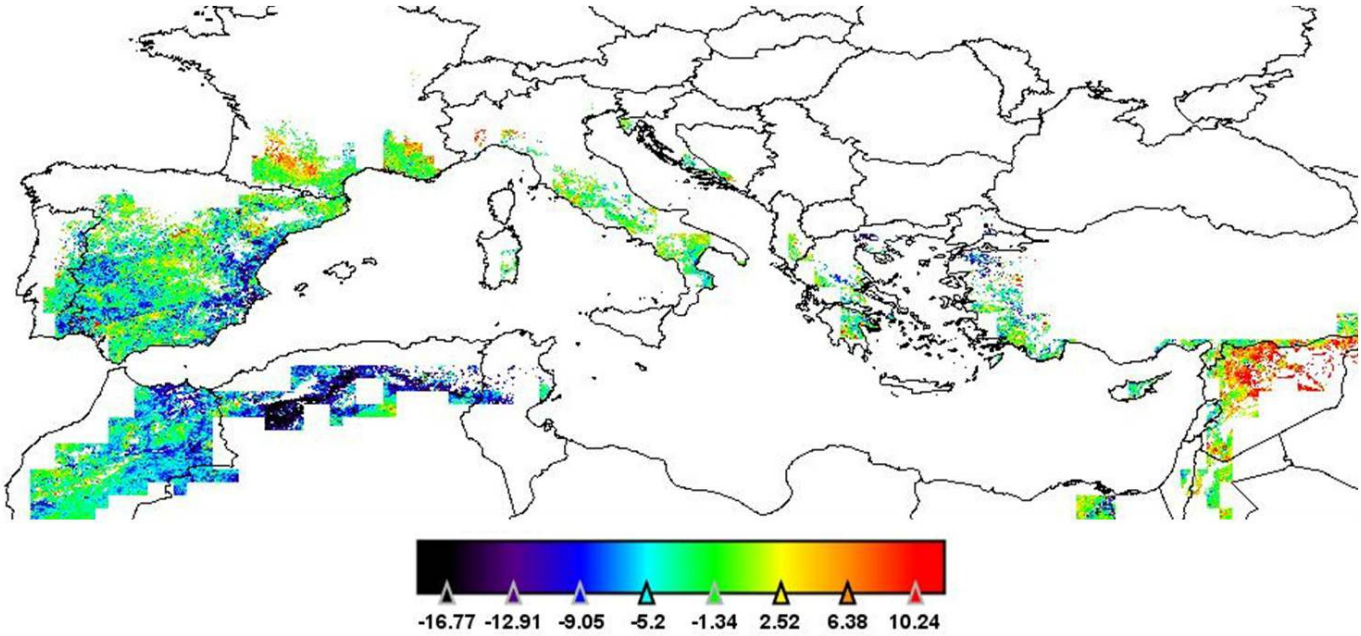

Figure 3. Spatial distribution of the LSA trends (in %) at the study area, computed for the period 2001-2012.

3.3 LSA trends vs. LC changes

As described in Section 2.4, an average LSA trend value was computed for every possible land cover change (including unchanged land cover types), that occurred in the study area during the period examined. These computations were based on statistically significant trends only, and the output is given in Table 2, whereby the first column shows the land cover type number (assigned in Table 1) in 2001 (initial land cover type), and the first row shows the final land cover type (in 2012). At least 100 pixels in each land cover change (cell in Table 2) were required for the average LSA change to be regarded representative. All LSA average changes are given in %, and the corresponding standard deviations are shown in parentheses.

The majority of average LSA changes in Table 2 is negative. The largest decreases of LSA occur when barren land changes to another land cover type (reduction of LSA by 10% or more). In fact, when barren land is converted to croplands, LSA decreases by 16.2% on average (the largest decrease found), while for the opposite land cover change, the largest increase in LSA is reported (13.6% on average). If LSA changes depended only on land cover changes, an opposite sign in LSA change would be expected in case of opposite land cover changes. This is not the case, however, in LSA average changes shown in Table 2. Furthermore, values of the main diagonal, which correspond to areas where land cover types remained unchanged, are also negative in the majority of land cover types. These findings, combined with the spatial distribution of LSA trends (Figure 3), which shows that LSA decreases dominate, imply that other factors also affect the LSA characteristics and evolution. The AOT may be one of these factors, its relationship with LSA, however, requires further investigation, beyond the scope of the present study. It may be also attributed to land management changes; that is anthropogenic modification without a change in land-cover type, as it has been recently described[17].

Table 2. Average LSA changes (in %) for each land cover change. The first column shows the initial land cover, and the first row shows the final land cover (see also Table 1 for land cover type numbers). Standard deviations of the average LSA changes are given in parentheses.

	1	**2**	**3**	**4**	**5**	**6**	**7**	**8**	**9**	**10**	**11**	**12**	**13**	**14**	**15**	**16**
1	0.6 (9.5)	-	-	-	1.7 (8.1)	-	-	11.0 (11.2)	-	-	-	-	-	-	-	-
2	-	-	-	-	-	-	-	-	-	-	-	-	-	-	-	-
3	-	-	-	-	-	-	-	-	-	-	-	-	-	-	-	-
4	-	-	-	-4.7 (4.0)	-4.1 (4.0)	-	-	-	-	-	-	-	-	-0.5 (7.2)	-	-
5	-1.6 (8.5)	-	-	-	-1.3 (6.6)	-	-	-1.0 (8.6)	-5.8 (7.3)	-	-	-1.3 (7.4)	-	-0.7 (7.1)	-	-
6	-4.5 (7.8)	-	-	-	-	-4.8 (6.6)	-2.4 (8.5)	-3.2 (7.7)	0.5 (8.9)	-	-	-	-	-	-	-
7	-	-	-	-	-	-9.3 (6.1)	-8.1 (7.6)	-9.4 (4.7)	-8.2 (3.8)	-8.1 (6.2)	-	-6.6 (6.1)	-	-7.2 (6.0)	-	-6.0 (11.3)
8	-5.9 (7.3)	-	-	-	-3.8 (6.3)	-5.3 (7.7)	-3.0 (11.2)	-5.3 (5.9)	-6.0 (7.0)	-1.4 (12.4)	-	-3.2 (7.9)	-	-3.6 (5.4)	-	-
9	-11.9 (17.0)	-	-	-	-5.8 (7.8)	-8.0 (8.8)	-3.3 (8.6)	-6.4 (5.3)	-7.2 (4.5)	-4.9 (7.9)	-	-6.3 (5.8)	-	-5.3 (4.6)	-	-
10	-	-	-	-	-5.5 (8.8)	-	-8.6 (7.3)	-7.2 (6.0)	-8.3 (3.9)	-6.4 (5.6)	-	-6.3 (5.3)	-	-5.1 (5.6)	-	-5.2 (10.3)
11	-	-	-	-	-	-	-	-	-	-	-	-	-	-	-	-
12	-	-	-	-	-6.4 (6.5)	-11.6 (12.3)	1.5 (9.3)	-7.0 (5.4)	-7.8 (4.6)	-5.9 (5.3)	-	-3.6 (7.0)	-	-5.0 (4.9)	-	13.6 (14.5)
13	-	-	-	-	-	-	-	-	-	-	-	-	-3.1 (7.0)	-	-	-
14	-	-	-	-	-4.4 (5.0)	-	-6.2 (19.8)	-4.9 (5.9)	-6.5 (3.5)	-4.6 (8.7)	-	-3.9 (6.6)	-	-3.3 (4.8)	-	-
15	-	-	-	-	-	-	-	-	-	-	-	-	-	-	-	-
16	-	-	-	-	-	-	-10.3 (7.2)	-	-	-9.2 (6.7)	-	-16.2 (11.8)	-	-	-	-5.2 (7.6)

4. SUMMARY AND CONCLUSIONS

The LSA was estimated at the climatically sensitive wider Mediterranean region, at 1 km × 1 km spatial resolution, for the period 2001-2012. For the estimation, 8-day satellite-derived products from MODIS were used, and the procedure comprised calculations of the black-sky and white-sky albedos, corresponding to direct and diffuse solar radiation, respectively, and their linear combination, also using data of the aerosol optical thickness and solar zenith angle. Based on the 8-day mean albedo, annual averages and corresponding trends were computed. The relationships between LSA characteristics and trends and corresponding land cover types and changes were also investigated.

Results showed that the highest albedo values (over 0.4) occur in barren areas, namely in deserts of northern Africa and the Middle East, while in southern Europe its values range between about 0.15 and 0.25. Large differences were found in the average LSA values for each land cover type, showing the importance of the latter in the LSA range.

Mixed signs of LSA trends were found at the study area, in several cases, however, large regions exhibit homogeneous behavior regarding the LSA changes. Overall, a tendency of decreasing LSA appears to dominate compared to corresponding increases. Investigation of LSA changes based on land cover changes also showed mainly decreasing trends, revealing that other factors, which require further investigation, also affect the LSA.

REFERENCES

[1] Dickinson, R. E., "Land surface processes and climate surface albedos and energy balance", Adv Geophys 25, 305-353 (1983).

[2] Shuai, Y., Masek, J. G., Gao, F. and Schaaf, C. B., "An algorithm for the retrieval of 30-m snow-free albedo from Landsat surface reflectance and MODIS BRDF", Remote Sens Environ 115, 2204-2216 (2011).

[3] Schaaf, C. B., Martonchik, J., Pinty, B., Govaerts, Y., Gao, F., Lattanzio, A., Liu, J., Strahler, A. and Taberner, M., "Retrieval of surface albedo from satellite sensors", In S. Liang (Ed.), Advances in land remote sensing: system, modeling, inversion and application, Springer, 219-243 (2008).

[4] Schaepman-Strub, G., Schaepman, M. E., Painter, T. H., Dangel, S. and Martonchik, J. V., "Reflectance quantities in optical remote sensing-definitions and case studies", Remote Sens Environ 103(1), 27-42 (2006).

[5] Liang, S., "Narrowband to broadband conversions of land surface albedo I: Algorithms", Remote Sens Environ 76, 213–238. (2000).

[6] Schaaf, C., Gao, F., Strahler, A., Lucht, W., Li, X., Tsung, T., Strugnell, N., Zhang, X., Jin, Y., Muller, J. P., Lewis, P., Barnsley, M., Hobson, P., Disney, M., Roberts, G., Dunderdale, M., Doll, C., d'Entremont, R., Hu, B., Liang, S., Previtte, J. and Roy, D., "First operational BRDF, albedo and nadir reflectance products from MODIS", Remote Sens Environ 83(1-2), 135-148 (2002).

[7] Trenberth, K. E., Jones, P. D., Ambenje, P., Bojariu, R., Easterling, D., Tank, A. K., Parker, D., Rahimzadeh, F., Renwick, J. A., Rusticucci, M., Soden, B. and Zhai, P., "Observations: Surface and Atmospheric Climate Change", In: Climate Change 2007: The Physical Science Basis. Contribution of Working Group I to the Fourth Assessment Report of the Intergovernmental Panel on Climate Change, edited by Solomon, S., Qin, D., Manning, M., Chen, Z., Marquis, M., Averyt, K. B., Tignor, M., Miller, H. L., Cambridge University Press, Cambridge, United Kingdom and New York, NY, USA, (2007).

[8] Trenberth, K. E., "Changes in precipitation with climate change", Clim Res 47, 123–138 (2011).

[9] IPCC, "Managing the Risks of Extreme Events and Disasters to Advance Climate Change Adaptation. A Special Report of Working Groups I and II of the Intergovernmental Panel on Climate Change", edited by Field, C. B., Barros, V., Stocker, T. F., Qin, D., Dokken, D. J., Ebi, K. L., Mastrandrea, M. D., Mach, K. J., Plattner, G. K., Allen, S. K., Tignor, M. and Midgley, P. M. Cambridge University Press, Cambridge, UK, and New York, NY, USA, 582 pp, (2012).

[10] Lucht, W., Schaaf, C. B. and Strahler, A. H., "An Algorithm for the Retrieval of Albedo from Space Using Semi empirical BRDF Models", IEEE Trans Geosci Remote Sensing 38(2), 977-998 (2000).

[11] Ross, J. K., "The radiation regime and architecture of plant stands", Springer Netherlands, The Netherlands, (1981).

[12] Roujean, J. L., Leroy, M. and Deschamps, P. Y., "A bi-directional reflectance model of the Earth's surface for the correction of remote sensing data", J Geophys Res 97(D18), 20455-20468 (1992).

[13] Li, X. and Strahler, A. H., "Geometric-optical bidirectional reflectance modeling of the discrete crown vegetation canopy: effect of crown shape and mutual shadowing", IEEE Trans Geosci Remote Sens 30, 276-292 (1992).

[14] Lewis, P. and Barnsley, M. J., "Influence of the sky radiance distribution on various formulations of the earth surface albedo", Proc Conf Phys Meas Sign Remote Sen, 707-715 (1994).

[15] Musial, J. P., Verstraete, M. M. and Gobron, N., "Technical Note: Comparing the effectiveness of recent algorithms to fill and smooth incomplete and noisy time series". Atmos Chem Phys 11, 7905-7923 (2011).

[16] Friedl, M. A., Sulla-Menashe, D., Tan, B., Schneider, A., Ramankutty, N., Sibley, A. and Huang, X., "MODIS Collection 5 global land cover: Algorithm refinements and characterization of new datasets". Remote Sens Environ 114(1), 168–182 (2010).

[17] Luyssaert, S. et al., "Land management and land-cover change have impacts of similar magnitude on surface temperature", Nature Clim Change 4, 389-393 (2014).